
A PSYCHOPHYSICAL ORIENTED SALIENCY MAP PREDICTION MODEL

Qiang LI

Image Processing Laboratory, Parc Cientific
University of Valencia
Valencia, 46980, Spain

qiang.li@uv.es

November 1, 2021

ABSTRACT

Visual attention is one of the most significant characteristics for selecting and understanding the outside redundancy world. The nature of complex scenes includes enormous redundancy. The human vision system can not process all information simultaneously because of visual information bottleneck. The human visual system mainly focuses on dominant parts of the scenes to reduce the input visual redundancy information. It is commonly known as visual attention prediction or visual saliency map. This paper proposes a new psychophysical saliency prediction architecture, WECSF, inspired by human low-level visual cortex function. The model consists of opponent color channels, wavelet transform, wavelet energy map, and contrast sensitivity function for extracting low-level image features and maximum approximation to the human visual system. The proposed model is evaluated several datasets, including MIT1003¹, MIT300², TORONTO³, SID4VAM⁴ and UCF Sports dataset⁵ to explain its efficiency. We also quantitatively and qualitatively compared the performance of saliency prediction with other state-of-the-art models. Our model achieved very stable and good performance. Second, we also confirmed that Fourier and spectral-inspired saliency prediction models achieved outperformance compared to other start-of-the-art non-neural networks and even deep neural network models on psychophysical synthesis images. Finally, the proposed model also can be applied to spatial-temporal saliency prediction and got better performance.

Keywords visual attention · redundancy · low-level visual cortex · opponent color channel · wavelet energy map · contrast sensitivity function · saliency prediction

1 Introduction

Visual attention is a significant perception function in the Human Vision System (HSV) to drive compact information from the complex nature scenes [Treisman and Gelade, 1980]. The nature scene images, including amount redundancy and usually useless for scene categories or recognition. Visual attention can extract essential features from redundant environment, which benefit visual information processing efficiency in the brain. The phenomenon of visual attention has been studied for a long time [Sun and Fisher, 2003]. Based on Barlow's *Efficiency Coding Hypothesis* [Barlow, 1959], visual attention has used to select relevant information and remove irrelevant information from redundant vision scenes. In general, there are two types of visual attention mechanisms: bottom-up and top-down branches. Bottom-up

¹<http://people.csail.mit.edu/tjudd/WherePeopleLook/index.html>

²<http://saliency.mit.edu/>

³<http://www-sop.inria.fr/members/Neil.Bruce/>

⁴http://www.cvc.uab.es/neurobit/?page_id=53

⁵https://www.crcv.ucf.edu/data/UCF_Sports_Action.php

models are mainly stimulus-driven. They are used to extract image features accompanied by visual information processing in the visual system, e.g., color, frequency, texture, orientation, and motion [Wang et al., 2005]. In contrast, the top-down approach, which is goal-driven, is usually high-level cognitive feedback and modulates low-level vision functional at a specific level [Itti, 2000]. In summary, both above computational neural modeling has been achieved application successfully in the saliency map prediction.

Many studies have tried to estimate bottom-up or top-down computational modeling to predict the saliency map. One of the earliest classical computational modelings was based on bottom-up mechanisms proposed by Itti et al. [Itti et al., 1998]. The model estimates the saliency map based on a human low-level vision system, and model structure contains linear filtering, center-surround differences, across-scale combinations, linear combinations. Achanta [Achanta et al., 2009] implemented a model for segmenting areas that producing high-resolution saliency maps for outstanding objects with clearly defined boundaries. Bruce and Tsotsos [Bruce and Tsotsos, 2005] suggested a model based on Shannon's measurement of self-information for saliency. They were performed in a neural system that demonstrated similar relations with the circuit in the primate's visual cortex. Li et al. [Li et al., 2012] proposed a new bottom-up model for identifying visual saliency based on an analysis of the amplitude spectrum of natural images. The saliency map is generated using the original phase and amplitude spectrum to reconstruct the 2D signal and filter it to a selected scale by minimizing salience entropy. Hou and Zhang [Hou and Zhang, 2008] introduced a dynamic visual attention model that is based on the rarity of features. They measured each feature's perspective entropy gain using the Incremental Coding Length (ICL). Murray et al. [Murray et al., 2011] demonstrated that an effective color appearance model in human vision, which involves a principled parameter selection as well as an innate spatial pooling function, can be extended to create a saliency model that outperforms state-of-the-art models. Zhang and Sclaroff [Zhang and Sclaroff, 2013] developed a new Boolean Map-based Saliency (BMS) model. BMS computes saliency maps by analyzing the topological structure of Boolean maps, which is based on the Gestalt principle of figure-ground segregation [Pinna et al., 2017]. Hou [Hou et al., 2011] introduced a simple image descriptor known as the image signature. They established a saliency algorithm based on the image signature to check if this estimated foreground overlaps with visually conspicuous image locations. Goferman [Goferman et al., 2010] presented a context-aware saliency method, which attempts to detect image regions that represent the scene. This definition varies from previous definitions in that its purpose is to detect the dominant object rather than to identify fixation points. Hou and Zhang [Hou and Zhang, 2007] demonstrated a straightforward approach for detecting perceptual saliency in objects that is unaffected by attributes, categories, or other types of prior information. They generate the corresponding saliency map in the spatial domain by evaluating an input image's log-spectrum. Guo [Guo et al., 2008] proposed a fast and straightforward Fourier transform-based approach called spectral residual (SR), which used SR of the amplitude spectrum to generate the saliency map. Schauerte and Stiefelhagen [Schauerte and Stiefelhagen, 2012] proposed using eigenaxes and eigenangles for quaternion Fourier transform-based spectral saliency models. Murray [Murray et al., 2013] proposed a saliency model based on a low-level spatiochromatic model that successfully predicted chromatic induction phenomena [Otazu et al., 2010]. Riche [Riche et al., 2012] proposed a new bottom-up model of visual saliency. It uses a sequential bottom-up feature extraction process. Low-level features, including luminance and chrominance, are computed first, and medium-level features such as image orientations are derived from the data. Duncan's Integrated Competition Hypothesis is presented by a novel object-based visual attention model that extends SUN [Zhang et al., 2008], and two new processes in the proposed model are identified and studied in depth. The first process determines the visual salience of points and groupings, while the second employs hierarchical sorting. Seo and Milanfar [Seo and Milanfar, 2009] presented a novel unified framework for detecting both static and space-time saliency. The "self-resemblance" calculation is then used to determine visual saliency. Spatterling [Spratling, 2011] proposed a saliency prediction model based on predictive coding theory, which is a subset of the predictive coding theory that has previously been shown to account for the response properties of orientation tuned cells in the primary visual cortex (V1) [Spratling, 2016]. As a result, this model offers a possible implementation of the hypothesis that V1 generates a bottom-up saliency map. Moreover, wavelet transform has also begun to be used to estimate the computational vision saliency map [Murray et al., 2011]. Compared to the Fourier Transform, it has a high resolution in both the frequency- and the time-domain. Wavelet transform can decompose signals on different scales, and it is also known as multi-resolution/multi-scale analysis or called sub-band coding that captures more low-level features from the original signal [Louis et al., 1997]. On the other hand, The wavelet transform approach can explain the primary visual cortex (V1) properties and produced multi-scale and multi-orientation features when given stimulus. The final saliency map estimated by sums up all the processed wavelet coefficients through inverse wavelet transform [Selvaraj and Shebiah, 2009]. The shortcomings of wavelet transform saliency map loss of global contract information rather than local contrast information.

In the last few years, some studies have tried to estimate the saliency map with deep convolutions neural networks (CNNs), and they have achieved impressive performances compared to conventional methods [Borji, 2019, Kruthiventi et al., 2016]. Cornia et al. [Cornia et al., 2016] introduced a novel deep architecture for saliency prediction. To predict saliency maps, current state-of-the-art models for saliency prediction use fully convolutional networks, which perform a non-linear combination of features extracted from the last convolutional layer. DeepGazeII [Kümmerer et al., 2016]

Models	Authors	Year	Inspiration
ITII	[Itti et al., 1998]	1998	Biological
Achanta	[Achanta et al., 2009]	2009	Fourier/Spectral
AIM	[Bruce and Tsotsos, 2005]	2005	Biological/Information-Theoretic
HFT	[li et al., 2012]	2013	Fourier/Spectral
ICL	[Hou and Zhang, 2008]	2008	Information-Theoretic
SIM	[Murray et al., 2011]	2011	Biological
BMS	[Zhang and Sclaroff, 2013]	2013	Probabilistic
DCTS	[Hou et al., 2011]	2011	Fourier/Spectral
CASD	[Goferman et al., 2010]	2010	Biological/Probabilistic
PFT	[Hou and Zhang, 2007]	2007	Fourier/Spectral
PQFT	[Guo et al., 2008]	2008	Fourier/Spectral
QDCT	[Schauerte and Stiefelhagen, 2012]	2012	Fourier/Spectral
SIMgrouping	[Murray et al., 2013]	2013	Biological/Cognitive
RARE	[Riche et al., 2012]	2012	Information-Theoretic
SUN	[Zhang et al., 2008]	2008	Probabilistic
SeoMilanfar	[Seo and Milanfar, 2009]	2009	Biological/Cognitive
Spratling	[Spratling, 2011]	2011	Biological/Cognitive
Simpsal	[Harel, 2012]	2012	Biological/Cognitive
ML_Net	[Cornia et al., 2016]	2016	Biological/Deep Neural Network
DeepGazeII	[Kümmerer et al., 2016]	2016	Biological/Deep Neural Network

Table 1: The prediction models for saliency. The names of the saliency prediction models are shown on the left side of the table. Model references are shown in the table’s center. The model function categories that inspired the developed corresponding models are shown on the right side of the table. Most saliency prediction models develop inspired by biological/cognitive, Fourier/spectral, information-theoretic, and probabilistic.

is a model that forecasts where people will look in images. The model employs features from the VGG-19 deep neural network, which has been trained to recognize objects in images. Compared to conventional methods, deep learning implantation easier to transfer to real-life applications, such as object detection, video understanding, and image compression. In short summary, all aforementioned of saliency prediction model summarize in the Tab. 1.

In this study, we proposed low-level human vision cortex inspired saliency prediction model. The model contains opponent color channels, wavelet energy map, and Contrast Sensitivity Function (CSF) components to predict human visual attention. The proposed model is bottom-up model and it evaluate with certain metrics, e.g., Area Under ROC Curve (AUC) [Borji et al., 2013], Normalized Scanpath Saliency (NSS) [Emami and Hoberock, 2013], Pearson’s Correlation Coefficient (CC) [Engelke et al., 2012], Similarity Intersection (SIM) [Riche et al., 2013], Kullback-Leibler divergence (KL) [Wilming et al., 2011], and Information Gain (IG) [Kümmerer et al., 2015b]. The details of the above metrics will introduce in Section 3. The proposed model was quantitatively evaluated with MIT1003, TORONTO and SID4VAM datasets compared with other different models.

The rest of this paper is organized as follows: Section II introduces the concept of opponent color space, wavelet decomposition, wavelet energy map estimation, and CSF. Section III introduced the model predict saliency map with different datasets and evaluating metrics from mathematics views. Section IV introduces the experiment results. The final section gives discussions and conclusions for the paper.

2 The Proposed Saliency Prediction Model

2.1 Saliency Prediction Model

The biologically inspired visual saliency prediction map is proposed based on the human low-level visual system. The extraction of information in the retina, LGN, and V1 is a critical component of visual neural networks. Color opponent channel, wavelet transform, wavelet energy map, and contrast sensitivity function were the main components of the proposed model architecture. The color opponent channel simulates retinal cells’ responses to different spectral wavelengths, and wavelet transforms presents multi-scale, multi-orientation properties of V1. The CSF is used to describe the human brain’s susceptibility to spatial frequency. The details of each component will be described in the following sections, respectively. The computational saliency prediction model architecture is illustrated in Fig. 1.

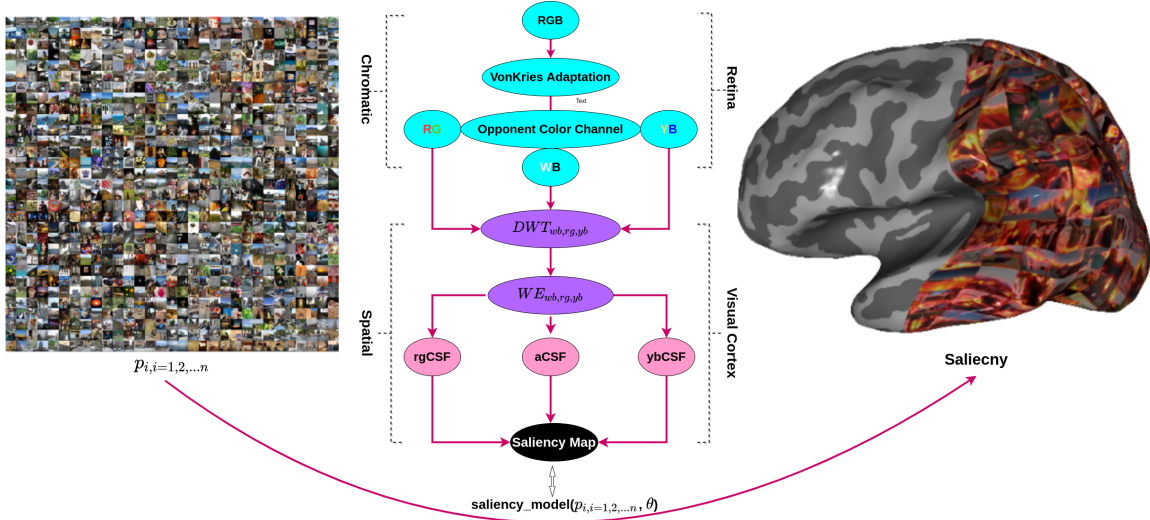


Figure 1: The architecture of proposed saliency prediction model. The left panel image was selected from the MIT1003 dataset. The middle graph shows a framework of the proposed model containing chromatic response in the retina and spatial feature processing in the visual cortex. The nature image was firstly adapted before decomposing into white-black, red-green, and yellow-blue opponent neural channels. In the spatial component, discrete wavelet transform is applied to each opponent’s color channel then wavelet energy map was measured. In the last step of the proposed model, the CSF is applied to each opponent’s wavelet energy channel and combined with each opponent’s feature. i and θ indicate image and parameters in the model, respectively. The details of each component were described in the following section. The right graph refers to the map left panel image saliency on the inflated visual cortex via the middle proposed model.

2.2 Gain control with von-Kries chromatic adaptation model

Gain control theory is widely used in cognitive psychology and is closely related to human dynamic behavior [Mercy, 1981]. Gain control exists in the visual information processing pipeline in the retina and cortex. In other words, gain control affects top-down and bottom-up visual information flow as well as attention-related cognitive function [Butz, 2004]. Meanwhile, the gain control always drives to maintain a steady-state brain and self-regulation condition between the brain and the natural environment. In the von-Kries model, we will multiply each channel of the image with gain value after normalizing its intensity [Finlayson et al., 1993, 2002, Krauskopf and Gegenfurtner, 1992]. However, note that there are some implications in this approach. The first one is that the channels are considered independent signals. That is why we have independent gains. Second, this gain is added not in the RGB space but the tristimulus LMS space. Assuming LMS corresponds to the tristimulus values of our image, and the von-Kries model mathematically can be expressed as:

$$L_2 = \frac{L_1}{L_{\max}} L_{\max 2}, M_2 = \frac{M_1}{M_{\max}} M_{\max 2}, S_2 = \frac{S_1}{S_{\max}} S_{\max 2} \quad (1)$$

$$\begin{bmatrix} L_{post} \\ M_{post} \\ S_{post} \end{bmatrix} = \begin{bmatrix} \frac{1}{L_{max}} & 0 & 0 \\ 0 & \frac{1}{M_{max}} & 0 \\ 0 & 0 & \frac{1}{S_{max}} \end{bmatrix} \begin{bmatrix} L_1 \\ M_1 \\ S_2 \end{bmatrix} \quad (2)$$

$$\begin{bmatrix} L_2 \\ M_2 \\ S_2 \end{bmatrix} = \begin{bmatrix} L_{max2} & 0 & 0 \\ 0 & M_{max2} & 0 \\ 0 & 0 & S_{max2} \end{bmatrix} \quad (3)$$

where L_1 corresponds to original images L values, L_{Max} , M_{Max} and S_{Max} corresponds to maximum value of each channel in the LMS image, L_{Max2} , M_{Max2} , and S_{Max2} are the gain value with setting value 0.6 in this proposed model, and L_2 is the corrected L channel after adaptation.

2.3 Color Appearance Model

The color opponent channel in the proposed model will be described in this section. Color representation in the brain can improve object recognition and identity while also reducing redundancy. As previously stated, visual information input from the natural environment contains significant redundancy [Barlow, 1990]. The Trichromatic Theory [Brill, 2014] and the color appearance model proposed, which is inspired by low-level human visual system function, helps us understand how the sensors encode color information and are widely used in low-level image processing. The two functional types of chromatic sensitivity or selectivity sensors were found: Single-Opponent and Double-Opponent neurons based on long (L), mediate (M), short (S) cones response in the physical light world [Shapley and Hawken, 2011](see Fig.2).

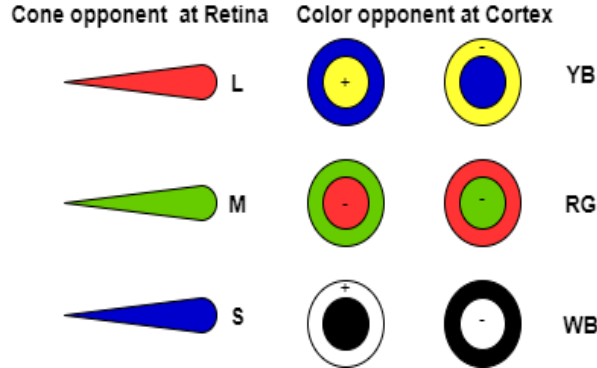


Figure 2: The receptive field of opponent color channel in the retina and visual cortex. L, M, and S refer to long, mediate, and short cones in the retina, and YB, RG, and WB indicate yellow-blue, red-green, and white-black opponent color channels, respectively. "+" indicates excitation, "-" represents inhibition.

The most of saliency predicts model used opponent color space is CIE Lab and YUV color spaces. In our case, we were introducing a new opponent color space proposed by Hering in 1957 [Hurvich and Jameson, 1957]. The color space transform matrix from RGB to $O_1O_2O_3$ can be expressed as:

$$\begin{bmatrix} O_1 \\ O_2 \\ O_3 \end{bmatrix} = \begin{bmatrix} 0.2814 & 0.6938 & 0.0638 \\ -0.0971 & 0.1458 & -0.0250 \\ -0.0930 & -0.2529 & 0.4665 \end{bmatrix} \begin{bmatrix} R \\ G \\ B \end{bmatrix} \quad (4)$$

The test nature scene images (size are 256x256, 512x512) were selected from Signal and Image Processing Institute, University of Southern California ⁶, and Kodak lossless true-color image database ⁷(size are 512x768, 768x512, 768x512). The total nature color images were resized into the same size (8 bits, 256x256) as test images. All nature chromatic images were converted from RGB space to ATD domain based on the above conversion matrix. As we see in Fig. 3, chromatic information (white-black, red-green, and yellow-blue) is decomposed into each channel.

⁶<http://sipi.usc.edu/database/database.php?volume=misc>

⁷<http://r0k.us/graphics/kodak/>

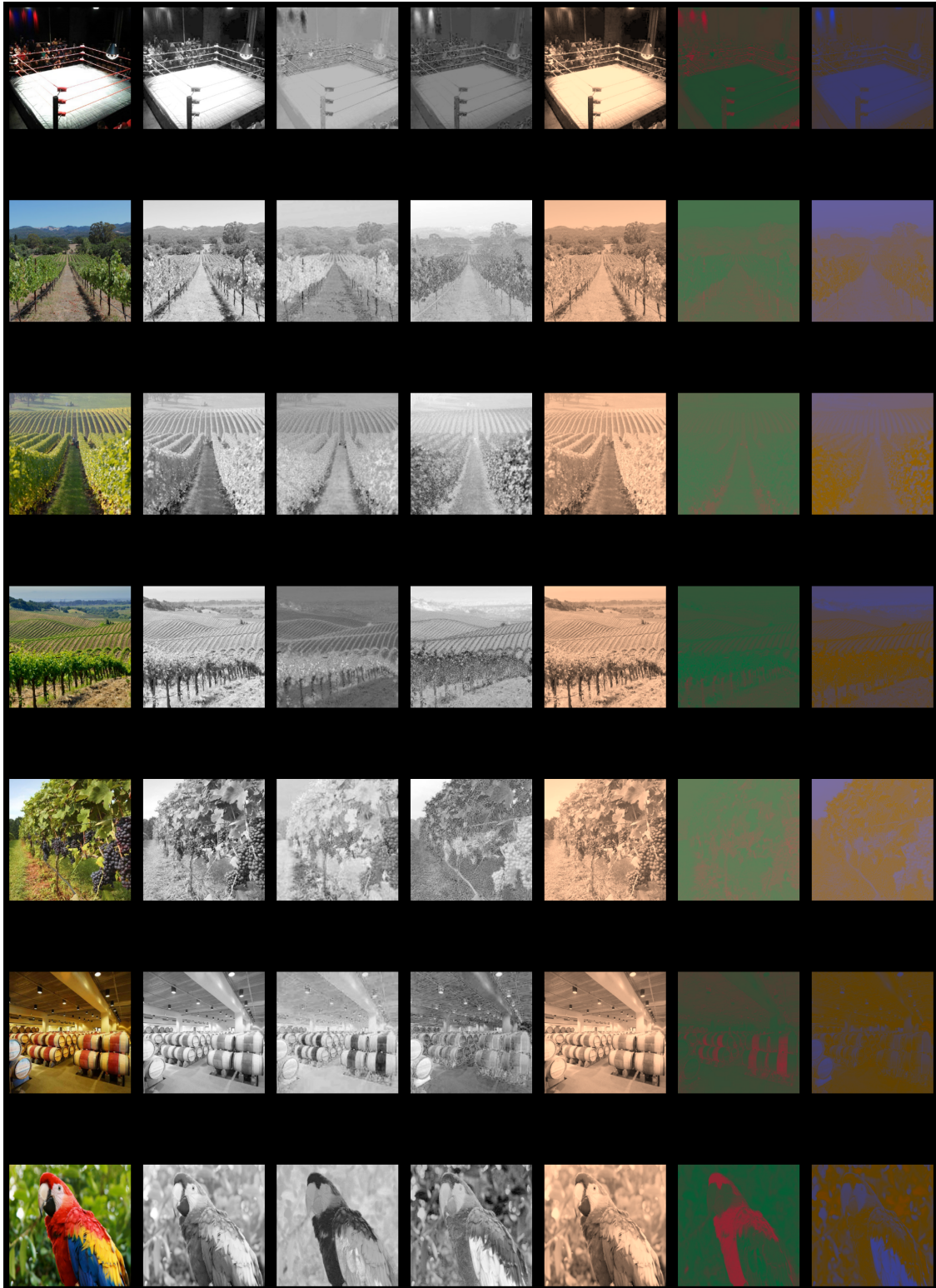


Figure 3: Opponent color processing. The first column represents the raw RGB color space, followed by the White-Black (WB) channel, Red-Green (RG) channel, and Yellow-Blue (YB) channel, each with a gray colormap. The final three columns depict the WB, RG, and YB channels in artificial color to better visualize opponent color processing at the visual cortex level.

2.4 Wavelet Energy Map

2.4.1 The visual cortex receptive fields with wavelet filters

The primary visual cortex contains neurons that reflect the structure of the retinal image in terms of a wavelet basis, and the visual simple and complex cells can be modeling with wavelet filters. In our case, we not considered in-depth details of each hyper-column neuron interactions mechanisms(e.g., Li's model [Zhaoping, 1998]). The V1 complex receptive fields simulated sum all squares of different scales and orientations after wavelet transform (see Fig.4). The V1 simple receptive fields in each opponent channel mathematically defined as:

$$V_{iv} = s_i o_v \tag{5}$$

$$V_{ih} = s_i o_h \tag{6}$$

$$V_{id} = s_i o_d \tag{7}$$

where s indicates receptive filed scales, o refers to orientation (e.g., vertical (v), horizontal (h), and diagonal (d), respectively) and i indicates number of neurons/features. Followed V1 complex cells can be formula as:

$$V_{complex} = \sum_1^i (s_i o_v)^2 + \sum_1^i (s_i o_h)^2 + \sum_1^i (s_i o_d)^2 \tag{8}$$

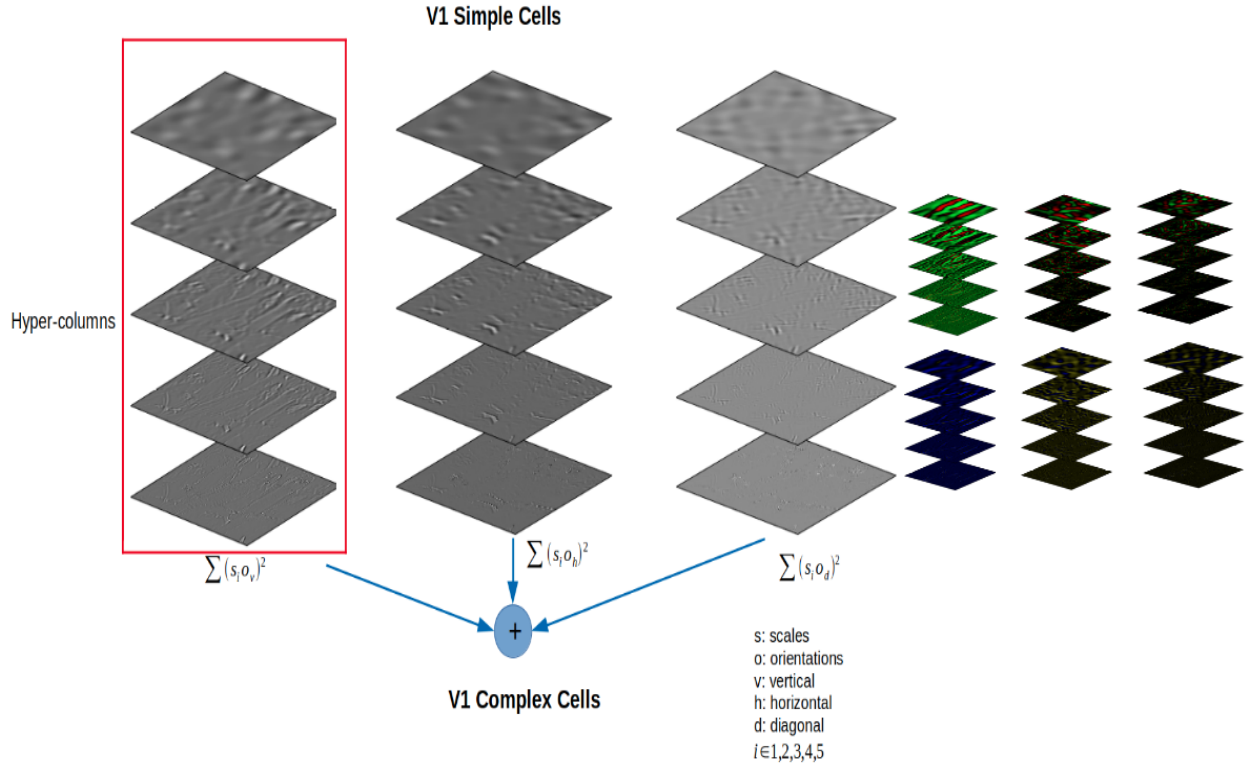


Figure 4: The modelling of V1 simple and complex cells in each opponent channel. The red vertical rectangle indicates hyper-columns in the visual cortex. From left to right graph depicts WB opponent neurons with different orientations and scales. The followed zoom out top/bottom graph with artificial color for better visualization of features in each hyper-column indicate RG/YB opponent neurons across different orientations and scales. The V1 complex cells can be obtained from the square of sum wavelet transform features across scales and orientations in the simple cells.

2.4.2 Wavelet transform and wavelet energy map

The wavelet image analysis can be decomposed image into multi-scale and multi-orientation features similar to visual cortex representation. Compared to the Fourier Transform (FT), wavelet transform can represent spatial and frequency information simultaneously. Alfred Haar first proposed the wavelet transform approach, and it has already been widely used in signal analysis [Haar, 1912], e.g., image compression, image denoising, classification. Wavelet transform was already applied in the visual saliency map prediction and achieved good performance [imamoğlu et al., 2013]. However, wavelet energy maps are still barely used in the visual saliency map prediction, and they can be used to enhance local contrast information in the decomposition sub-bands. Discrete wavelet transform (DWT) used in our proposed model, and it can be mathematically expressed as:

$$r[n] = ((I * f)[n]) \downarrow 2 = \left(\sum_{k=-\infty}^{\infty} I[k]f[n-k] \right) \downarrow 2 \quad (9)$$

where I indicates input images, f represents a series of filter banks (low-pass and high-pass), and $\downarrow 2$ indicates down-sampling until the next layer signal cannot be decomposed any more (see Fig. 5). A series of sub-band images are produced after convolution with DWT, and then wavelet energy map can be calculated from each sub-band features (see Fig. 6).

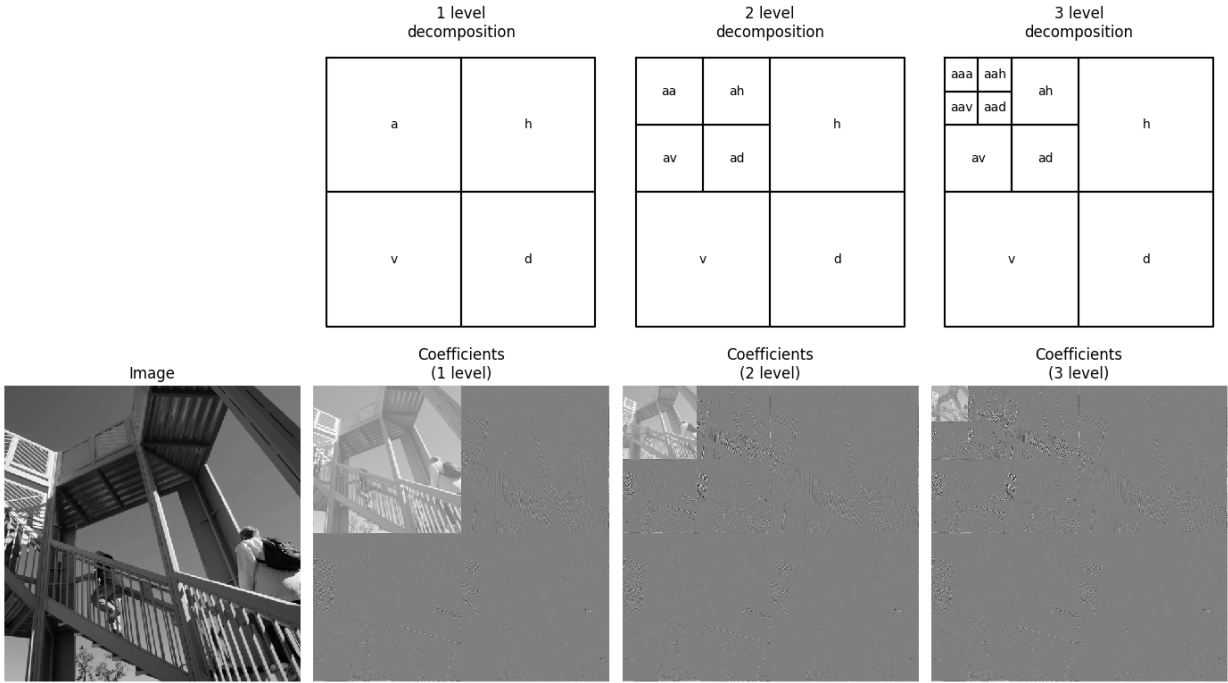


Figure 5: The different decomposition levels with DWT. e.g., 1 level, 2 level and 3 level. 'a' indicates original image, 'h' indicates horizontal feature, 'v' refers vertical feature, and 'd' represents diagonal feature, respectively. The bottom left image refers to the original image and then follows images representing 1, 2, and 3 level decomposition features from the original image.

The wavelet energy map can be expressed as:

$$\mathcal{WE}(i, j) = \|I(i, j)\|^2 = \sum_{k=1}^{3ind+1} |I_k(i, j)|^2 \quad (10)$$

where ind indicates the maximum level of an image can be decomposed in the last, and $I_k(i, j)^2$ represents the energy map of each sub-band features.

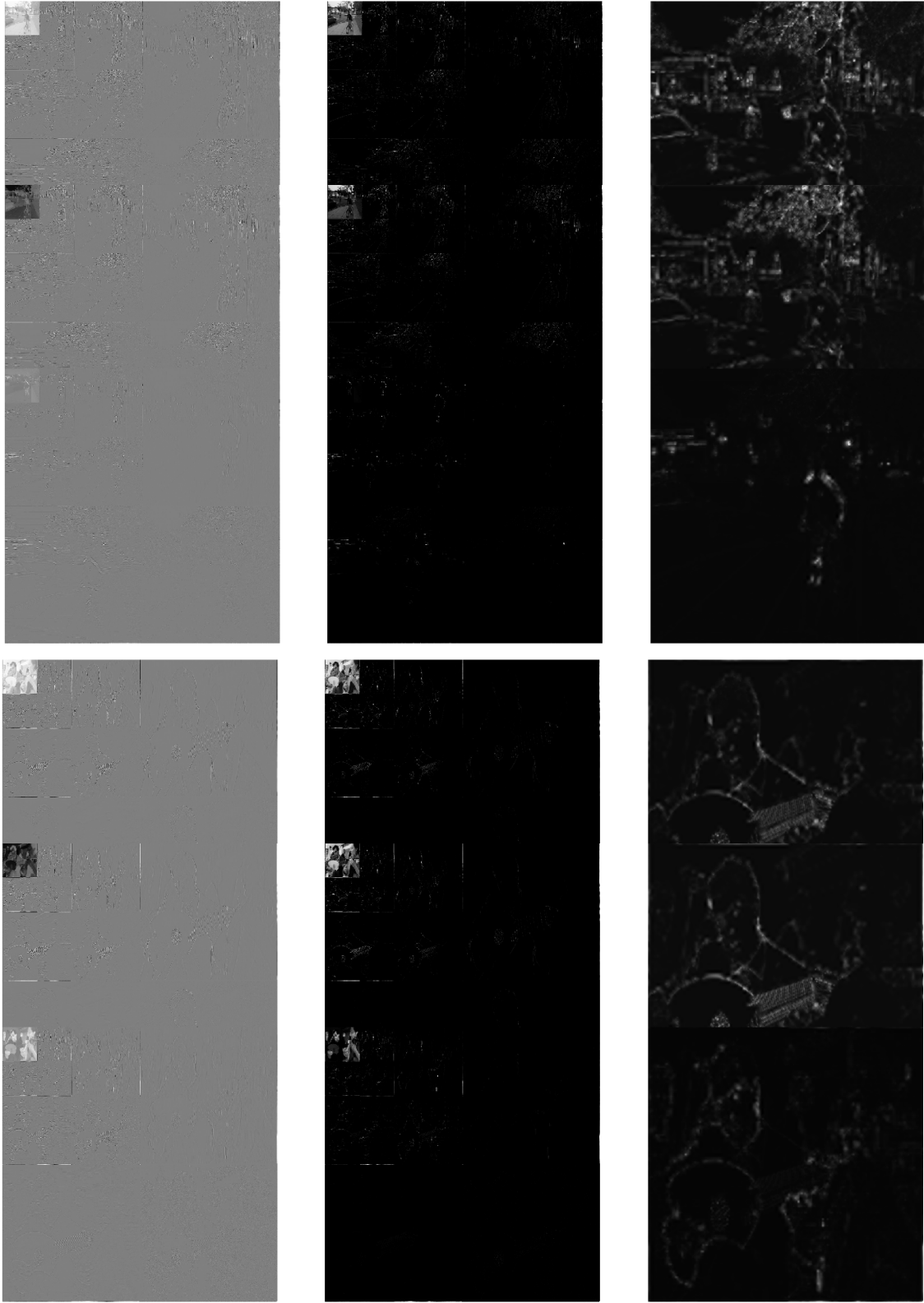


Figure 6: Each channel's DWT map and the wavelet energy maps correspond to it. The first column refers to DWT maps for achromatic (WB) and chromatic(RG, YB) channels. The second column indicates the wavelet energy map via sum across scales and orientation features for WB, RG, and YB opponent channels, respectively. The last column represents the squared of sum energy maps in each opponent channel.

2.5 Contrast Sensivity Function

The human visual system is compassionate of contrast change in the natural environment. The visual cortex function can be decomposed into subset compositions, and one of the significant features is CSF. It can be divided into achromatic and chromatic spatial CSFs [Mullen, 1985]. In this proposed computational modeling, achromatic CSF (aCSF) and chromatic CSFs (rgCSF and ybCSF) were implemented into the model, which was firstly proposed by Mannos and Sakrison in 1974 [Mannos and Sakrison, 1974] then improved later [Watson and Malo, 2002, Watson and Ahumada, 2010] (see Fig. 7). The achromatic CSF mathematics can be expressed as:

$$CSF(f_x, f_y) = Q(f) * L(f_x, f_y) \quad (11)$$

$$Q(f) = g * (\exp(-(f/f_m)) - l * \exp(- (f^2/s^2))) \quad (12)$$

$$L(f_x, f_y) = 1 - w * (4(1 - \exp(-(f/os))) * f_x^2 * f_y^2 / f^4) \quad (13)$$

where (f_x, f_y) indicates 2D spatial frequency vector (in cycle/deg), f represents modulus of the spatial frequency (cycle/deg), g represents overall gain ($g = 330.74$), f_m indicates parameter that control the exponent decay of the CSF Tyler ($f_m = 7.28$), l represents loss at low frequencies ($l = 0.837$), s indicates parameter that control the attenuation of the loss factor at high frequencies ($s = 1.809$), w indicates weighting of the Oblique Effect ($w = 1$), os indicates Oblique Effect scale ($os = 6.664$).

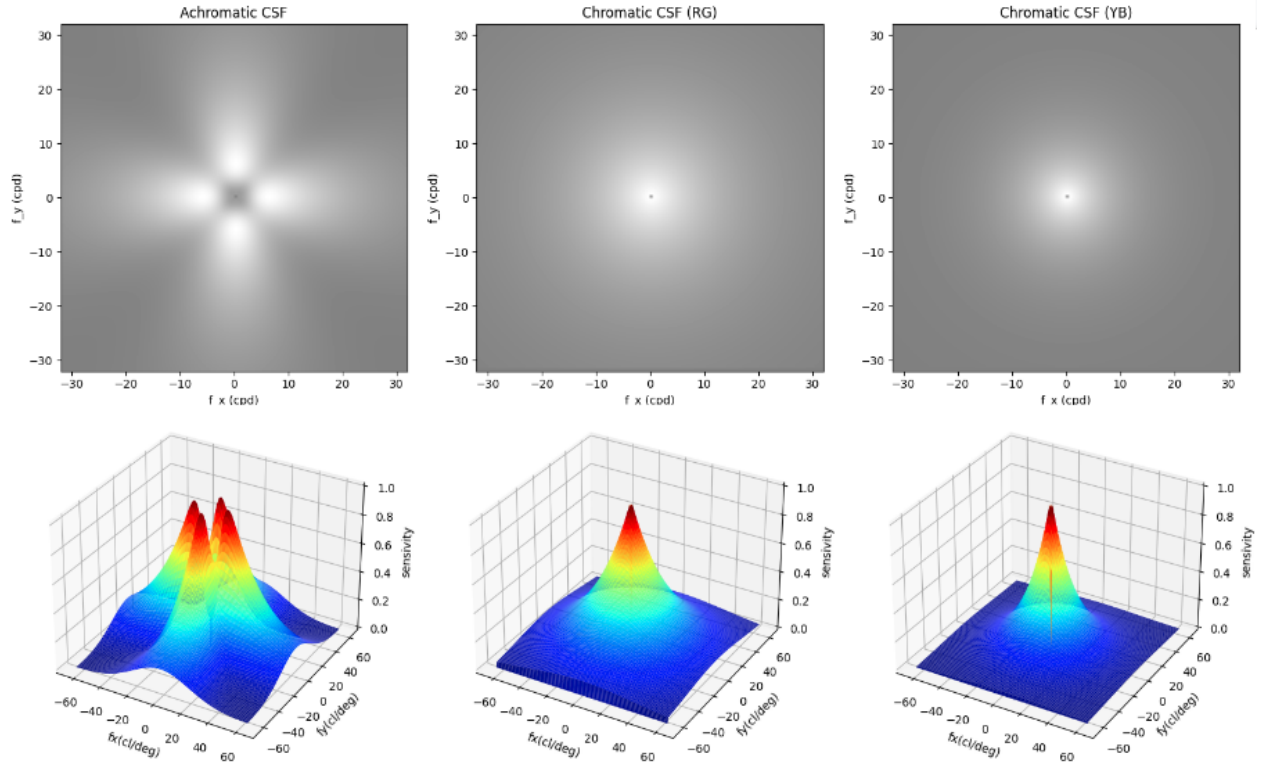


Figure 7: Achromatic and Chromatic CSF. The top image refers to 2D CSFs and bottom row indicates 3D CSFs.

The CSF is applied with the wavelet energy image in the Fourier domains. It can be the formula as:

$$CSF_{WE} = \text{real}(\mathcal{F}(\mathcal{I}(\mathcal{I}(\mathcal{F}(WE.\text{real}))) \otimes CSF)) \quad (14)$$

where F indicates 2D Fourier transform, \mathcal{F} indicates 2D inverse Fourier transform, I indicates *fftshift* and \mathcal{I} indicates *ifftshift*. The Python implementation of above CSFs (aCSF, rgCSF and ybCSF) are available at <https://github.com/sinodanishspain/CSFpy>.

3 Materials and Methods

3.1 Datasets

The proposed model was tested on several well-known datasets, including MIT1003, MIT300, TORONTO, and SID4VAM. The basic information of each dataset will be introduced as follows.

3.1.1 MIT1003

MIT1003 is an image dataset that includes 1003 images from the Flickr and LabelMe collections (see Fig. 8). The fixation map was generated from recording 15 participants' eye-tracking data. It is the largest eye tracking dataset. The dataset includes 779 landscapes and 228 portraits of images which size spanning from 405×405 to 1024×1024 pixels [Judd et al., 2012].

3.1.2 MIT300

MIT300 is a benchmark saliency test dataset that includes 300 images from recoding 39 observers' eye-tracking dataset (see Fig. 8). The MIT300 dataset categories are highly varied and natural. The dataset can be used for model evaluation [Judd et al., 2012].



Figure 8: MIT1003 (left panel image) and MIT300 datasets (right panel image).

3.1.3 TORONTO

The TORONTO dataset included 120 chromatic images and was free-viewed by 20 subjects (see Fig. 9). The datasets contained both outdoor and indoor scenes with a fixed resolution of 511×681 pixels [Bruce and Tsotsos, 2005].

3.1.4 SID4VAM

SID4VAM is a synthetic image database that is mainly used to psycho-physical evaluate the V1 properties (see Fig. 9). The database is composed of 230 synthetic images. It includes 15 distinct types of low-level features (e.g., brightness, size, color, and orientation.) with different a target-distractor pop-out type of synthetic images [Berga et al., 2019].



Figure 9: TORONTO (left panel image) and SID4VAM (right panel image) datasets.

3.2 Evaluation Metrics

There are several approaches, as we mentioned before, to evaluate metrics between visual saliency and model prediction. In general, saliency evaluation can be divided into two branches that location-based and distribution-based respective. The former mainly focuses on the district located in the saliency map, and the latter considers both predicted saliency and human eye fixation maps as continuous distributions [Bylinskii et al., 2016]. In this research, we used AUC, NSS, CC, SIM, IG, and KL to evaluate methods and details of each evaluation metric described as follows⁸.

3.2.1 Area under ROC Curve (AUC)

The AUC metric is one of the popular approaches to evaluate saliency model performances. The saliency map can be treated as a binary classifier to split positive samples from negative samples by setting different thresholds. The actual positive (TP) is the saliency map values' proportion beyond a specific threshold at the fixation locations. In verse, the positive (FP) is the saliency map values' proportion beyond a specific threshold at the non fixation locations. In our case, the thresholds are set from the saliency map values and AUC-Judd, AUC-Borji and sAUC measured [Borji et al., 2013].

3.2.2 Normalized Scanpath Saliency (NSS)

The NSS metric usually measured the relationship between human eye fixation maps and model prediction saliency maps [Emami and Hoberock, 2013]. Given a binary fixation map F and saliency map S , the NSS can be formally defined as:

$$NSS = \frac{1}{N} \sum_{i=1}^N \bar{S}(i) x F(i) \quad (15)$$

$$N = \sum_i F(i) \text{ and } \bar{S} = \frac{S - \mu(S)}{\sigma(S)} \quad (16)$$

where N is the total number of human eye positions, $\mu(s)$ is mean value of saliency maps and $\sigma(S)$ is the standard deviation.

⁸<https://github.com/cvzoya/saliency>

3.2.3 Similarity Metric (SIM)

The similarity metric (SIM) is a very famous algorithm from measure image structure similarity, and it has already widely used in image quality and image processing disciplines [Riche et al., 2013]. The SIM mainly measured the normalized probability distributions of eye fixation and model prediction saliency maps. The SIM can be mathematically described as:

$$SIM = \sum_{i=1} \min(P(i), Q(i)) \quad (17)$$

where $P(i)$ and $Q(i)$ are the normalized saliency map and the fixation map, respectively. A similarity score should be located between zero and one.

3.2.4 Information Gain (IG)

The information gain is an approach to measure saliency map prediction accuracy from the information-theoretic view. It mainly measured the critical information contained in the predict saliency map compared with the ground truth map [Kümmerer et al., 2015a]. The mathematical formula of IG can be expressed as:

$$IG(P, Q^B) = \frac{1}{N} \sum_i Q_i^B [\log_2(\epsilon + P_i) - \log_2(\epsilon + B_i)] \quad (18)$$

where P indicate prediction saliency map, and Q^B is baseline map, ϵ represents regularity parameters.

3.2.5 Pearson's Correlation Coefficient (CC)

Pearson's Correlation Coefficient (CC) is one of the linear approaches that measured how many similarities between prediction saliency map and baseline map [Jost et al., 2005].

$$CC(P, Q^D) = \frac{\sigma(P, Q^D)}{\sigma(P) \times \sigma(Q^D)} \quad (19)$$

where P indicates prediction saliency map and Q^D is the ground truth saliency map.

3.2.6 Kullback-Leibler divergence (KL)

The Kullback-Leibler divergence (KL) was used to measure two distribution samples' distance from information-theoretic views [Kümmerer et al., 2015a]. It can be formally defined as:

$$KL(P, Q^D) = \sum_i Q_i^D \log \left(\epsilon + \frac{Q_i^D}{\epsilon + P_i} \right) \quad (20)$$

where P indicates prediction saliency map and Q^D is the ground truth saliency map. ϵ also represents regularity parameters.

3.2.7 Other metrics

We also evaluate different salient prediction models' performance through two main metrics, including the precision-recall curves (PR curves), F-measure⁹. By binarizing the predicted saliency map with thresholds in [0,255], a series of precision and recall score pairs is calculated for each dataset image. The PR curve is plotted using the average precision and recall of the dataset at different thresholds either [Feng, 2018].

⁹https://github.com/ArcherFMY/sal_eval_toolbox/

4 Experimental Results

4.1 Quantitative Comparison of the Proposed Model with other State-of-the-Art Models

To evaluate the performance of the proposed model, we compared it with the other eight state-of-the-art models. We selected MIT1003 and SID4VAM benchmarks for a comparison of the quantitative results. These results were reported in Tab. 2, Tab. 3 and Tab. 4. The better performance on the saliency prediction is biological/cognitive and Fourier/spectral inspired models. Our model got stable better performance over different from evaluating metrics compared to other biological/cognitive and Fourier/spectral inspired models. However, saliency map prediction based on convolution neural network got outperformed than other models in nature scene images because it feeds larger images to training neural networks. Consequently, it cannot be compared to other models because it is based on more statistics principles than neuroscience. In this paper, we emphasize understanding saliency prediction from neuroscience perspective and further help us understand the mechanism of visual attention cognitive function. Furthermore, biological/cognitive and Fourier/spectral inspired saliency detection models got outperformed then deep learning (ML_Net and DeepGazeII) in the SID4VAM dataset (see Tab. 4 and Fig. 13). As previously said, SID4VAM is a synthetic image database that is primarily used to psycho-physically test the VI properties, which is also why we stated that deep learning models result from more statistics than neuroscience in the explanation of human visual attention mechanisms.

Methods	DNN	AUC_Judd	AUC_Borji	sAUC	NSS	SIM
ITT	B	0.674	0.655	0.610	0.629	0.291
WECSF	N	0.705	0.692	0.653	0.849	0.362
SR	N	0.708	0.683	0.638	0.791	0.329
AIM	N	0.706	0.696	0.639	0.780	0.282
BMS	N	0.684	0.637	0.576	0.729	0.346
CASD	N	0.747	0.731	0.651	0.977	0.350
DCTS	N	0.746	0.732	0.650	1.000	0.322
HFT	N	0.797	0.764	0.619	1.258	0.416
ICL	N	0.769	0.713	0.617	1.048	0.420
PFT	N	0.708	0.683	0.636	0.787	0.326
PQFT	N	0.643	0.530	0.519	0.459	0.292
QDCT	N	0.736	0.714	0.647	0.920	0.338
RARE	N	0.777	0.755	0.665	1.198	0.380
SIM	N	0.701	0.693	0.653	0.743	0.283
SUN	N	0.665	0.647	0.601	0.629	0.287
Achanta	N	0.534	0.526	0.526	0.174	0.240
Simpsal	N	0.735	0.721	0.610	0.892	0.337
Spratling	N	0.512	0.508	0.510	0.039	0.234
SIMgrouping	N	0.724	0.716	0.668	0.873	0.308
SeoMilanfar	N	0.710	0.688	0.633	0.808	0.351
ML_Net	Y	0.836	0.743	0.689	1.928	0.565
DeepGazeII	Y	0.886	0.837	0.779	2.483	0.527

Table 2: Quantitative scores of several models for the MIT1003 dataset. The baseline ITT model are SkyBlue-hatched and proposed model are Green-hatched. The black bold scores indicate best performance of saliency prediction models. 'N' indicates NO and vice versa, 'B' indicate Baseline. The results of MIT1003 dataset of ML_Net and DeepGazeII are pink-hatched because the dataset is used to train ML_Net and DeepGazeII and cannot be compared with other models.

4.2 Qualitative Comparison of the Proposed Model with Other State-of-the-Art Models

We qualitatively tested the proposed model with the MIT1003, MIT300, TORONTO, SID4VAM and UCF Sports dataset, respectively. Meanwhile, we compared the model performance with other state-of-the-art saliency prediction modelings on the MIT1003, TORONTO and SID4VAM datasets. Fig. 10, Fig. 11, Fig. 12, Fig. 13 and Fig. 14 illustrate the saliency map results obtained when the proposed model and other state-of-the-art models are applied to sample images drawn from the studied dataset. The performance of each of saliency prediction models evaluate with AUC and PR curves in the Fig.15. We can see that the proposed model can predict most of the salient objects in the given images. Furthermore, the proposed model can successfully detect the orientation, boundary, and pop out function when the model applied the SID4VAM dataset. In summary, our proposed biological/Fourier/spectral inspired saliency prediction

Methods	DNN	AUC_Judd	AUC_Borji	sAUC	NSS	SIM
ITT	B	0.700	0.679	0.641	0.816	0.317
WECSF	N	0.701	0.686	0.674	0.844	0.365
SR	N	0.744	0.722	0.683	1.019	0.343
AIM	N	0.727	0.718	0.664	0.885	0.356
SIM	N	0.754	0.744	0.707	0.951	0.361
SUN	N	0.674	0.653	0.613	0.656	0.285
HFT	N	0.820	0.792	0.659	1.548	0.522
ICL	N	0.792	0.737	0.652	1.245	0.532
PFT	N	0.742	0.717	0.684	1.001	0.339
CASD	N	0.780	0.764	0.688	1.237	0.364
PQFT	N	0.650	0.524	0.517	0.482	0.263
QDCT	N	0.769	0.748	0.691	1.174	0.354
RARE	N	0.806	0.774	0.693	1.514	0.402
Achanta	N	0.551	0.541	0.539	0.249	0.305
Simpsal	N	0.769	0.754	0.648	1.121	0.355
Spratling	N	0.508	0.503	0.509	0.015	0.242
SIMgrouping	N	0.769	0.760	0.710	1.090	0.326
SeoMilanfar	N	0.769	0.744	0.695	1.185	0.382
ML_Net	Y	0.823	0.803	0.750	1.824	0.536
DeepGazeII	Y	0.846	0.827	0.756	2.199	0.620

Table 3: Quantitative scores of several models for the Toronto dataset. The baseline ITT model are SkyBlue-hatched and proposed model are Green-hatched. The black bold scores indicate best performance of saliency prediction models. The results of Toronto dataset of ML_Net and DeepGazeII are pink-hatched because the dataset is used to train ML_Net and DeepGazeII and cannot be compared with other models either.

Models	DNN	AUC_Judd	AUC_Borji	sAUC	CC	NSS	KL	SIM	IG
GT	B	0.943	0.882	0.860	1.000	4.204	0.000	1.000	2.802
Baseline-CG	B	0.703	0.697	0.525	0.281	1.577	0.722	0.372	-0.189
ITT	B	0.645	0.592	0.591	0.165	0.801	1.778	0.315	-0.104
WECSF	N	0.667	0.647	0.646	0.378	1.019	1.769	0.459	-1.508
AIM	N	0.572	0.566	0.560	0.118	0.515	14.96	0.216	-18.742
Achanta	N	0.505	0.513	0.513	0.060	0.334	8.431	0.117	-9.634
BMS	N	0.811	0.517	0.515	0.129	0.702	19.161	0.624	-24.258
CASD	N	0.737	0.673	0.663	0.429	2.124	2.659	0.397	-1.263
DCTS	N	0.732	0.725	0.715	0.440	2.191	1.442	0.377	0.363
HFT	N	0.780	0.753	0.697	0.561	2.364	1.424	0.458	0.406
ICL	N	0.742	0.716	0.630	0.344	1.189	1.974	0.391	-0.443
PFT	N	0.704	0.692	0.688	0.407	2.074	2.556	0.361	-1.230
PQFT	N	0.581	0.518	0.517	0.112	0.611	12.262	0.175	-15.074
QDCT	N	0.717	0.705	0.699	0.419	2.139	1.850	0.368	-0.213
SIM	N	0.648	0.638	0.628	0.181	0.744	1.799	0.340	-0.152
SR	N	0.747	0.695	0.689	0.423	2.087	1.508	0.414	0.354
SUN	N	0.545	0.536	0.535	0.086	0.403	17.387	0.155	-22.268
Simpsal	N	0.753	0.740	0.661	0.370	1.380	1.461	0.393	0.323
Spratling	N	0.535	0.527	0.534	0.030	0.176	17.801	0.147	-22.890
SIMgrouping	N	0.649	0.638	0.638	0.191	0.866	1.925	0.350	-0.338
SeoMilanfar	N	0.703	0.692	0.698	0.246	1.181	2.696	0.337	-1.400
ML_Net	Y	0.600	0.593	0.501	0.118	0.341	7.529	0.370	-2.153
DeepGazeII	Y	0.645	0.581	0.475	0.103	0.555	2.450	0.274	-1.128

Table 4: Quantitative scores of several models for the SID4VAM dataset. The baseline ITT model are LightBlue-hatched and proposed model are Green-hatched. The black bold scores indicate best performance of saliency prediction models. The Fourier/Spectral inspired models has the best prediction scores compared to other start-of-the-art non-neural network and even deep neural network models on the SID4VAM dataset. The results of SID4VAM dataset of ML_Net and DeepGazeII are pink-hatched because the dataset is used to train ML_Net and DeepGazeII and cannot be compared with other models either.

model got better stable performances over nature images, psycho-physicals synthesis images, and dynamic scenes compared with other models.



Figure 10: Performance evaluation with MIT1003 database. The first row is color image, second row is ground truth saliency map and the last row is proposed model prediction saliency map, respectively.

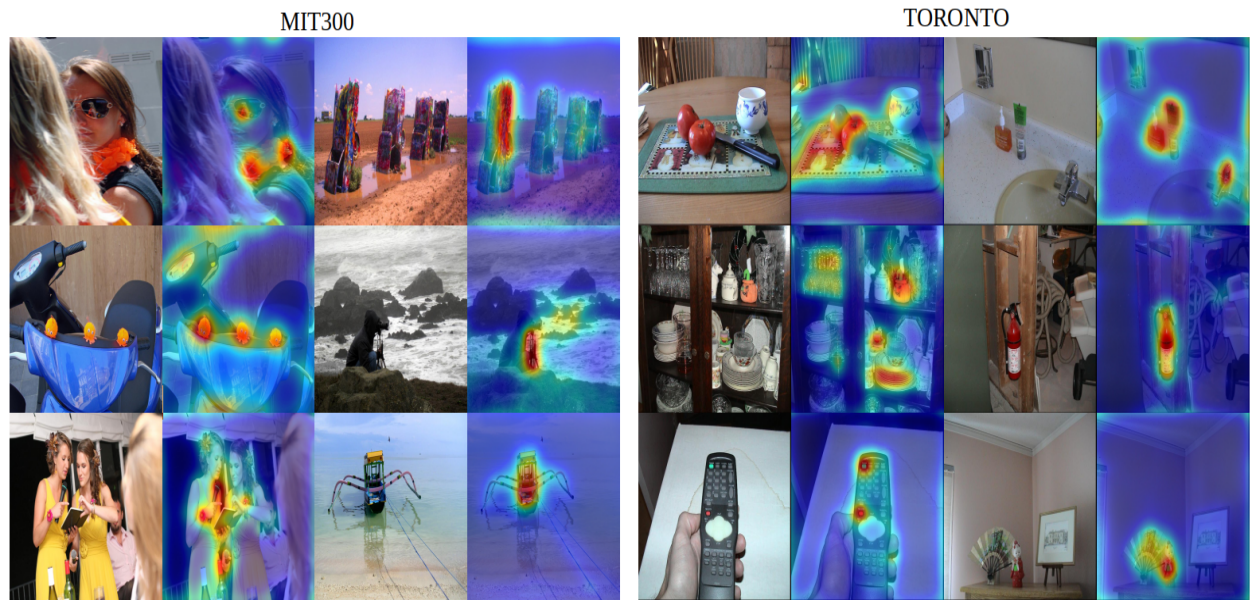


Figure 11: Left:Performance evaluation with MIT300 database. The first and third column are color images. The second and fourth column are proposed model prediction saliency maps. Right:Performance evaluation with TORONTO database. The first and third column are color images. The second and fourth column are proposed model prediction saliency maps.

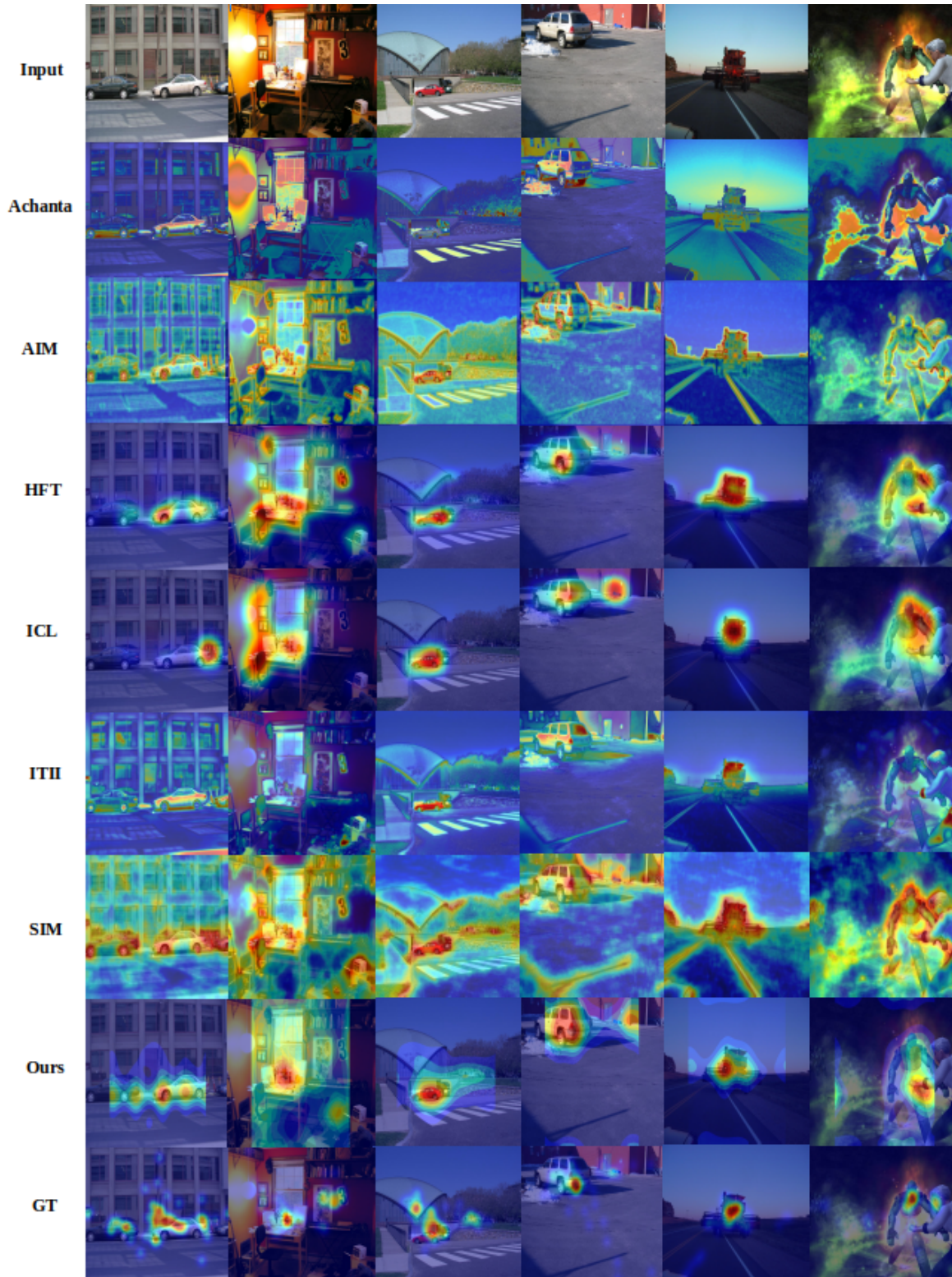


Figure 12: Qualitative saliency prediction results from MIT1003 database with selected different models. The first row is six stimuli images selected from the MIT1003 database. Then follow with Achanta, AIM, HFT, ICL, ITII, SIM, Proposed models, and Ground Truth (GT) saliency prediction result with artificial color for better visualization.

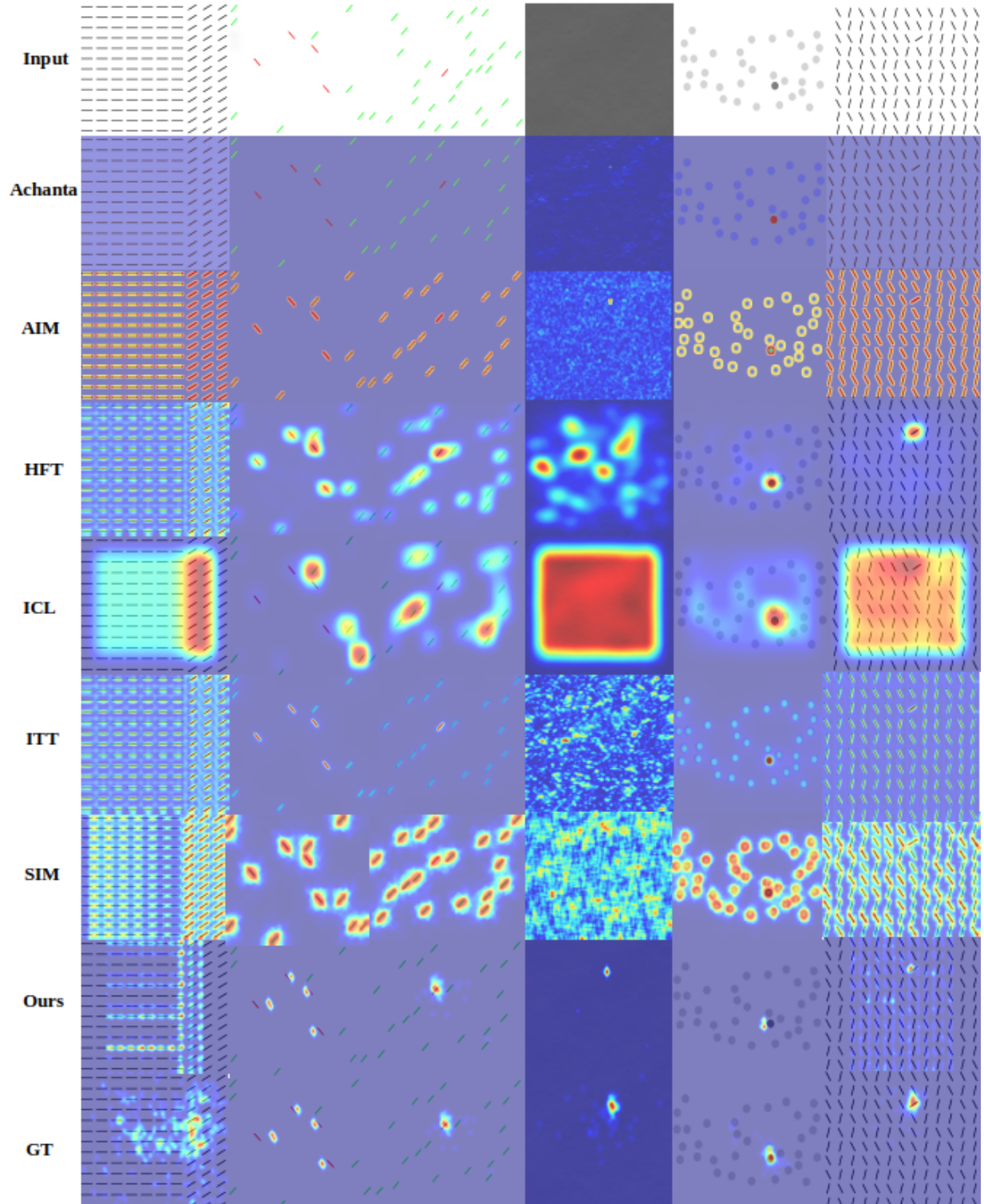


Figure 13: Qualitative saliency prediction results from SID4VAM database with selected different models. The first row is six stimuli images selected from the SID4VAM database. Then follow with Achanta, AIM, HFT, ICL, ITT, SIM, Proposed models, and Ground Truth (GT) saliency prediction result with artificial color for better visualization. The proposal model can be successfully applied to explain "pop out" effect in visual search.

Frames=1:28

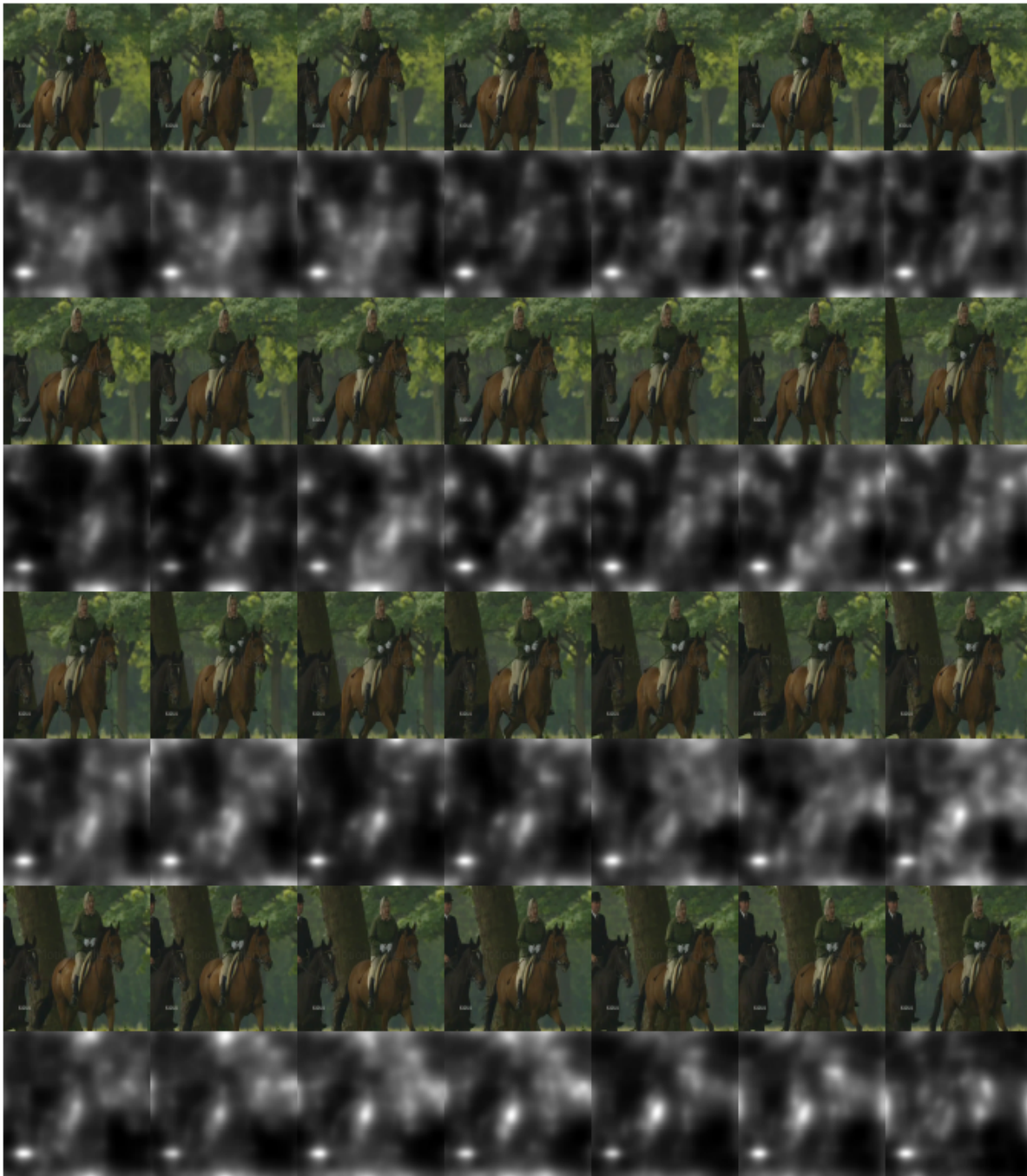


Figure 14: Dynamic saliency prediction. For these sample frames from UCF Sports Action Dataset. The model clearly produces better results and perfectly captures the left-bottom text information.

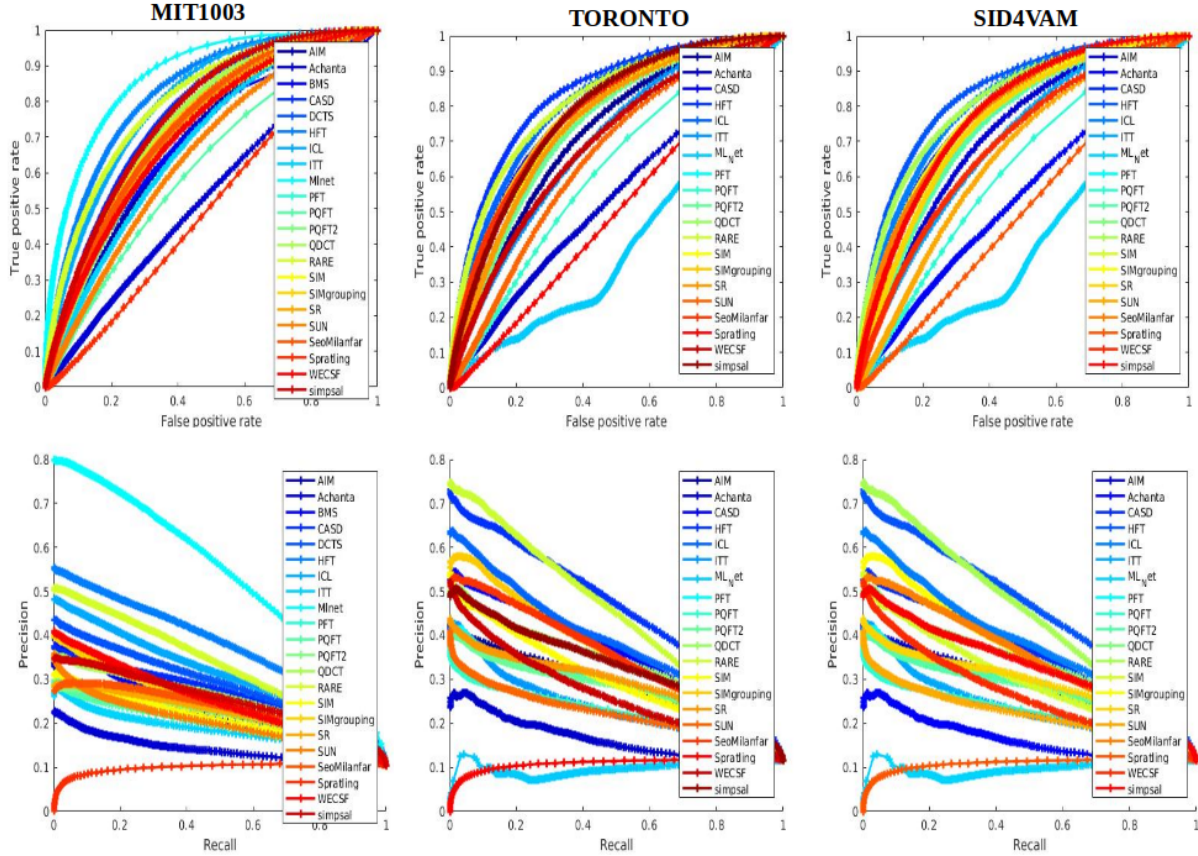


Figure 15: Comparison of the area-under-the-curve (AUC) and PR curves with different thresholds of our method and other state-of-art methods on three benchmark datasets.

5 Discussion

Saliency modeling has already become a hot research topic between computer vision and neuroscience. Therefore, we are simply always trying new architectures that are not enough to improve model performance. Instead, we should investigate how humans perceive scenes; what guides their attention is critical. In this article, I'll discuss several ways to go beyond the capabilities of models.

First, we need to understand the cognitive attention mechanism. Visual attention is a selective cognitive process that allows us to deal effectively with this issue by choosing important information and filtering out irrelevant information. In saliency prediction studies, spatial attention plays a significant role in the discriminability and appearance task, and it is affected by spatial resolution and contrast sensitivity. Exploring visual attention neural mechanisms can help us develop better and more accurate saliency prediction models. In contrast, better saliency prediction models also can help us understand the visual attention cognitive process in the brain. Second, we need multi-model and multi-label datasets to evaluate saliency prediction model performance. The domain dataset used to assess the saliency prediction model is the MIT Saliency benchmark datasets. As we mentioned before, the saliency prediction model should not only purely get higher accuracy on the nature scene images but also on the psychophysical synthesis images, e.g., SID4VAM. It can help us improve the model architecture and also help us understand the cognitive attention process. Third, we have provided comprehensive experimental results that show that our method consistently got stable and better performances than other state-of-the-art methods in the previous section. It's worth noting that we measure saliency using biologically visual model estimation. Our proposed saliency prediction model takes more neuroscience concepts into account rather than probability/statistics. Furthermore, we have a few parameters in the proposed model, and they are largely set and fixed for all experiments. Using wavelet energy maps and opponent CSFs as features is one of the most critical factors that make the proposed method more efficient. Furthermore, our comprehensive experimental results indicate that the proposed saliency prediction measure derived from a local image energy estimator is much more effective

and straightforward than other existing methods. Although our method is built entirely on biologically computational principles, the resulting model structure exhibits considerable agreement with the fixation behavior of the human visual system.

6 Conclusions

This study proposed a computational psychophysical visual saliency prediction model inspired by a low-level human visual pathway. The model includes color opponent channel, wavelet transform, wavelet energy map, and contrast sensitivity functions to predict saliency map. The model was evaluated by classical benchmark datasets and achieved stable and good performance of visual saliency prediction compared with the baseline model. Furthermore, we found that deep neural network outperforms nature image salient prediction but underperforms psychophysical synthesis images. In contrast, Fourier/Spectral inspired model has the opposite effect because Fourier/Spectral inspired model simulates optical neural processing from the retina to V1. However, the deep neural network takes statistics into account more than low-level vision system function. Finally, we also extend our model to spatial-temporal saliency prediction, and it can capture the most significant feature in the videos.

7 Acknowledgments

We thank the anonymous reviewers whose suggestions helped improve and clarify this manuscript. This research received no external funding.

8 Conflicts of Interest

The authors declare no conflicts of interest.

9 Abbreviations

HSV	Human Vision System
V1	Primary Visual Cortex
ICL	Incremental Coding Length
CNN	Convolution Neural Network
DNN	Deep Neural Network
WT	Wavelet Transform
IWT	Inverse Wavelet Transform
AUC	Area under ROC curve
NSS	Normalized Scanpath Saliency
CC	Pearson's Correlation Coefficient
SIM	Similarity or histogram intersection
IG	InformationGain
KL	Kullback–Leibler divergence
CSF	Contrast Sensitivity Function
FT	Fourier Transform
DWT	Discrete Wavelet Transform
IDWT	Inverse Discrete Wavelet Transform
LGN	Lateral Geniculate Nucleus
GT	Ground Truth

References

- R. Achanta, S. Hemami, F. Estrada, and S. Süsstrunk. Frequency-tuned salient region detection. *Proceedings of the IEEE Conference on Computer Vision Pattern Recognition (CVPR)*, 06 2009.
- H. Barlow. Sensory mechanisms, the reduction of redundancy, and intelligence. *Proc. of the Nat. Phys. Lab. Symposium on the Mechanization of Thought Process*, (10):535–539, 1959.
- H. Barlow. *Vision: Coding and Efficiency*, chapter A theory about the functional role and synaptic mechanism of visual aftereffects. Cambridge Univ. Press, Cambridge, UK, 1990.

- D. Berga, X. R. Fdez-Vidal, X. Otazu, and X. M. Pardo. Sid4vam: A benchmark dataset with synthetic images for visual attention modeling. *2019 IEEE/CVF International Conference on Computer Vision (ICCV)*, pages 8788–8797, 2019.
- A. Borji. Saliency prediction in the deep learning era: Successes and limitations. *IEEE transactions on pattern analysis and machine intelligence*, PP, 08 2019.
- A. Borji, H. Rezazadegan Tavakoli, D. Sihite, and L. Itti. Analysis of scores, datasets, and models in visual saliency prediction. pages 921–928, 12 2013.
- M. Brill. *Trichromatic Theory*, pages 827–829. 01 2014. ISBN 978-0-387-30771-8.
- N. D. B. Bruce and J. K. Tsotsos. Saliency based on information maximization. In *Proceedings of the 18th International Conference on Neural Information Processing Systems, NIPS’05*, page 155–162, Cambridge, MA, USA, 2005. MIT Press.
- M. Butz. Toward a cognitive sequence learner: Hierarchy, self-organization, and top-down bottom-up interaction. 04 2004.
- Z. Bylinskii, T. Judd, A. Oliva, A. Torralba, and F. Durand. What do different evaluation metrics tell us about saliency models? *arXiv preprint arXiv:1604.03605*, 2016.
- M. Cornia, L. Baraldi, G. Serra, and R. Cucchiara. A deep multi-level network for saliency prediction. 09 2016.
- M. Emami and L. Hoberock. Selection of a best metric and evaluation of bottom-up visual saliency models. *Image and Vision Computing*, 31:796–808, 10 2013.
- U. Engelke, H. Liu, J. Wang, P. Le Callet, I. Heynderickx, H.-J. Zepernick, and A. Maeder. A comparative study of fixation density maps. *IEEE transactions on image processing : a publication of the IEEE Signal Processing Society*, 11 2012.
- M. Feng. Evaluation toolbox for salient object detection. https://github.com/ArcherFMY/sal_eval_toolbox, 2018.
- G. Finlayson, M. Drew, and B. Funt. Color constancy: Enhancing von kries adaptation via sensor transformations. *Proc SPIE*, 1913, 09 1993.
- G. D. Finlayson, A. Alsam, and S. D. Hordley. Local linear models for improved von kries adaptation. In *The Tenth Color Imaging Conference: Color Science and Engineering Systems, Technologies, Applications, CIC 2002, Scottsdale, Arizona, USA, November 12-15, 2002*, pages 139–144. IS&T - The Society for Imaging Science and Technology, 2002.
- S. Goferman, L. Zelnik-Manor, and A. Tal. Context-aware saliency detection. pages 2376 – 2383, 07 2010.
- C. Guo, Q. Ma, and L. Zhang. Spatio-temporal saliency detection using phase spectrum of quaternion fourier transform. 06 2008.
- A. Haar. Zur theorie der orthogonalen funktionensysteme. (zweite mitteilung). *Mathematische Annalen*, 71:38–53, 1912. URL <http://eudml.org/doc/158516>.
- J. Harel. A saliency implementation in matlab. <http://www.klab.caltech.edu/~harel/share/gbvs.php>, 2012.
- X. Hou and L. Zhang. Saliency detection: A spectral residual approach. volume 2007, 06 2007.
- X. Hou and L. Zhang. Dynamic visual attention: Searching for coding length increments. volume 21, pages 681–688, 01 2008.
- X. Hou, J. Harel, and C. Koch. Image signature: Highlighting sparse salient regions. *IEEE transactions on pattern analysis and machine intelligence*, 34, 07 2011.
- L. Hurvich and D. Jameson. An opponent-process theory of color vision. *Psychological Review*, 64:384–404, 12 1957.
- N. imamoğlu, W. Lin, and Y. Fang. A saliency detection model using low-level features based on wavelet transform. *IEEE Transactions on Multimedia*, 15:96–105, 01 2013.
- L. Itti. *Models of Bottom-Up and Top-Down Visual Attention*. PhD thesis, Pasadena, California, Jan 2000.
- L. Itti, C. Koch, and E. Niebur. A model of saliency-based visual attention for rapid scene analysis. *Pattern Analysis and Machine Intelligence, IEEE Transactions on*, 20:1254 – 1259, 12 1998.
- T. Jost, N. Ouerhani, R. Wartburg, R. Müri, and H. Hügli. Assessing the contribution of color in visual attention. *comput. vis. image und.* 100, 107-123. *Computer Vision and Image Understanding*, 100:107–123, 10 2005.
- T. Judd, F. Durand, and A. Torralba. A benchmark of computational models of saliency to predict human fixations. In *MIT Technical Report*, 2012.
- J. Krauskopf and K. Gegenfurtner. Color discrimination and adaptation. *Vision research*, 32:2165–75, 12 1992.

- S. Kruthiventi, V. Gudisa, J. Dholakiya, and R. Babu. Saliency unified: A deep architecture for simultaneous eye fixation prediction and salient object segmentation. pages 5781–5790, 06 2016.
- M. Kümmerer, T. S. A. Wallis, and M. Bethge. Deepgaze II: reading fixations from deep features trained on object recognition. *CoRR*, abs/1610.01563, 2016. URL <http://arxiv.org/abs/1610.01563>.
- M. Kümmerer, T. Wallis, and M. Bethge. Information-theoretic model comparison unifies saliency metrics. *Proceedings of the National Academy of Sciences*, 112:201510393, 12 2015a.
- M. Kümmerer, T. Wallis, and M. Bethge. Information-theoretic model comparison unifies saliency metrics. *Proceedings of the National Academy of Sciences*, 112:201510393, 12 2015b.
- J. li, M. Levine, X. An, X. Xu, and H. He. Visual saliency based on scale-space analysis in the frequency domain. *IEEE Transactions on Pattern Analysis and Machine Intelligence*, 35:996–1010, 11 2012.
- A. Louis, P. Maass, and A. Rieder. *Wavelets: Theory and Applications*. 01 1997. ISBN 978-0-471-96792-7.
- J. Mannos and D. Sakrison. The effects of a visual fidelity criterion of the encoding of images. *IEEE Transactions on Information Theory*, 20(4):525–536, 1974.
- D. Mercy. A review of automatic gain control theory. *Radio and Electronic Engineer*, 51, 01 1981.
- K. Mullen. The contrast sensitivity of human color vision to red-green and blue-yellow chromatic gratings. *The Journal of physiology*, 359:381–400, 03 1985.
- N. Murray, M. Vanrell, X. Otazu, and C. A. Párraga. Saliency estimation using a non-parametric low-level vision model. pages 433–440, 06 2011.
- N. Murray, M. Vanrell, X. Otazu, and C. A. Párraga. Low-level spatiochromatic grouping for saliency estimation. *IEEE transactions on pattern analysis and machine intelligence*, 35:2810–6, 11 2013.
- X. Otazu, C. A. Párraga, and M. Vanrell. Toward a unified chromatic induction model. *Journal of vision*, 10:5, 10 2010.
- B. Pinna, A. Reeves, J. Koenderink, A. Doorn, and K. Deiana. A new principle of figure-ground segregation: The accentuation. *Vision research*, 143, 12 2017.
- N. Riche, M. Mancas, B. Gosselin, and T. Dutoit. Rare: A new bottom-up saliency model. 10 2012.
- N. Riche, M. Duvinage, M. Mancas, B. Gosselin, and T. Dutoit. Saliency and human fixations: State-of-the-art and study of comparison metrics. 12 2013.
- B. Schauerte and R. Stiefelhagen. Quaternion-based spectral saliency detection for eye fixation prediction. pages 116–129, 10 2012. ISBN 978-3-642-33708-6.
- A. Selvaraj and N. Shebiah. Object recognition using wavelet based salient points. *The Open Signal Processing Journal*, 2:14–20, 09 2009.
- H. Seo and P. Milanfar. Static and space-time visual saliency detection by self-resemblance. *Journal of vision*, 9: 15.1–27, 11 2009.
- R. Shapley and M. Hawken. Color in the cortex: Single- and double-opponent cells. *Vision research*, 51:701–17, 02 2011.
- M. Spratling. Predictive coding as a model of the v1 saliency map hypothesis. *Neural networks : the official journal of the International Neural Network Society*, 26:7–28, 10 2011.
- M. Spratling. A review of predictive coding algorithms. *Brain and Cognition*, 112, 01 2016.
- Y. Sun and R. Fisher. Object-based visual attention for computer vision. *Artificial Intelligence*, 146:77–123, 05 2003.
- A. Treisman and G. Gelade. A feature-integration theory of attention. *Cognitive psychology*, 12:97–136, 02 1980.
- D. Wang, A. Kristjansson, and K. Nakayama. Efficient visual search without top-down or bottom-up guidance. *Perception & psychophysics*, 67:239–53, 03 2005.
- A. Watson and A. Ahumada. The spatial standard observer. *Journal of Vision - J VISION*, 4:51–51, 01 2010.
- A. Watson and J. Malo. Video quality measures based on the standard spatial observer. volume 3, pages III–41, 02 2002. ISBN 0-7803-7622-6.
- N. Wilming, T. Betz, T. Kietzmann, and P. König. Measures and limits of models of fixation selection. *PloS one*, 6: e24038, 09 2011.
- J. Zhang and S. Sclaroff. Saliency detection: A boolean map approach. pages 153–160, 12 2013.
- L. Zhang, M. Tong, T. Marks, H. Shan, and G. Cottrell. Sun: A bayesian framework for saliency using nature statistics. *Journal of vision*, 8:32.1–20, 02 2008.
- L. Zhaoping. A neural model of contour integration in the primary visual cortex. *Neural computation*, 10:903–40, 05 1998.